ELSEVIER

Physics of the Earth and Planetary Interiors 118 (2000) 29–51

PHYSICS OF THE EARTH AND PLANETARY INTERIORS

www.elsevier.com/locate/pepi

Rayleigh–wave tomography of the Ontong–Java Plateau

W. Philip Richardson [a,b], Emile A. Okal [a,*], Suzan Van der Lee [c,d]

[a] *Department of Geological Sciences, Northwestern University, 1847 Sheridan Road, Evanston, IL 60201, USA*
[b] *Chevron Petroleum Technology, 935 Gravier Street, New Orleans, LA 70112, USA*
[c] *Department of Terrestrial Magnetism, Carnegie Institution of Washington, 5241 Broad Brach Road, N.W., Washington, DC 20015, USA*
[d] *Institut für Geophysik, Eidgenössische Technische Hochschule, Hönggerberg, CH-8093 Zürich, Switzerland*

Received 6 April 1999; accepted 6 July 1999

Abstract

The deep structure of the Ontong–Java Plateau (OJP) in the westcentral Pacific is investigated through a 2-year deployment of four PASSCAL seismic stations used in a passive tomographic experiment. Single-path inversions of 230 Rayleigh waveforms from 140 earthquakes mainly located in the Solomon Trench confirm the presence of an extremely thick crust, with an average depth to the Mohorovičić discontinuity of 33 km. The thickest crusts (38 km) are found in the southcentral part of the plateau, around 2°S, 157°E. Lesser values remaining much thicker than average oceanic crust (15–26 km) are found on either side of the main structure, suggesting that the OJP spills over into the Lyra Basin to the west. Such thick crustal structures are consistent with formation of the plateau at the Pacific–Phoenix ridge at 121 Ma, while its easternmost part may have formed later (90 Ma) on more mature lithosphere. Single-path inversions also reveal a strongly developed low-velocity zone at asthenospheric depths in the mantle. A three-dimensional tomographic inversion resolves a low-velocity root of the OJP extending as deep as 300 km, with shear velocity deficiencies of $\sim 5\%$, suggesting the presence of a keel, dragged along with the plateau as the latter moves as part of the drift of the Pacific plate over the mantle.

Keywords: Ontong–Java Plateau; Rayleigh waveform; Solomon Trench

1. Introduction and background

We present the results of a 2-year passive tomographic experiment over the Ontong–Java Plateau (OJP), a massive feature of the western Pacific Basin, located between the Caroline Islands to the north and the Solomon Islands to the south (Fig. 1). The plateau is generally L-shaped, with the horizontal arm of the ''L'' extending into the south Nauru Basin. It rises an average of 2000 m above the basin floor, reaching soundings of less than 4000 m over an area of 1.6×10^6 km^2, and culminating at 2000 m below sea level in its southcentral section, around 3°S, 157°E. This makes the OJP the largest ''Large Igneous Province'' (LIP) on Earth. These provinces have generally been described as resulting from rapid episodes of massive basaltic flooding (Coffin and Eldholm, 1994), and as such may be conceptually similar to planetary structures such as the lunar maria, the Tharsis region of Mars, the Beta–Atla–Themis Province of Venus, and possibly the smooth

* Corresponding author. Tel.: +1-847-491-3194; fax: +1-847-491-8060; e-mail: emile@earth.nwu.edu

0031-9201/00/$ - see front matter
PII: S0031-9201(99)00122-3

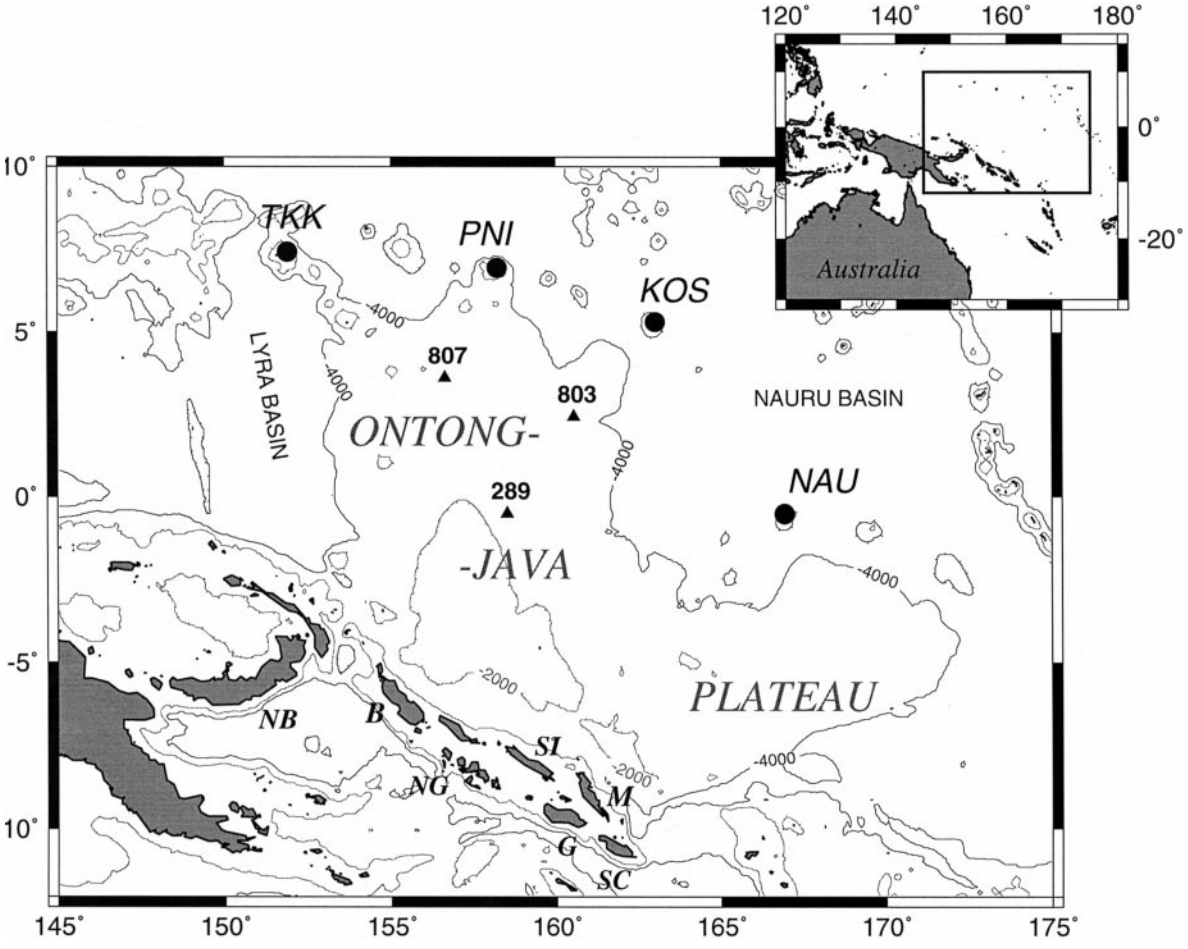

Fig. 1. Location map for the OJP seismic experiment. The plateau is defined by the 4000-m isobath (labeled); the 2000-m one is also shown. The four island stations deployed are shown as solid circles, with three-letter codes: TKK (Chuuk), PNI (Pohnpei), KOS (Kosrae) and NAU (Nauru). The triangles show the DSDP/ODP sites where drilling returned basaltic samples. The following islands mentioned in the text are identified: Malaita (M), Santa Isabel (SI), San Cristobal (SC), Guadalcanal (G), New Georgia (NG), Bougainville (B) and New Britain (NB). Ramos is a small islet between Malaita and Santa Isabel which cannot appear on the scale of this figure. The inset replaces the main map (box) in the local geographical context.

plains of Mercury (Head and Coffin, 1997), although significant differences exist among the topographic expressions and the rates of extrusion on each planet.

Such massive eruptions must involve relatively violent episodes of accelerated mantle dynamics, themselves representative of major changes in the pace of the Earth's internal engine, and in turn potentially impacting its surficial environment. However, the exact association, and causal relationship between LIP eruptions and such disruptions as the onset of the magnetic quiet interval, or the Cretaceous extinctions, remain highly speculative (e.g., Sleep, 1990; Arthur et al., 1991; Larson, 1991; Larson and Olson, 1991; Head and Coffin, 1997). In this general framework, the investigation of LIPs is of prime importance to our improved understanding of the internal dynamics of the Earth and its sister planets.

In very general terms, two classes of models have been proposed to explain the origin of LIPs, following ideas originally put forth by Morgan (1981). In the *passive* model, LIPs are generated during conti-

nental rifting over a zone of permanent upwelling (White and McKenzie, 1989, 1995). In the *active* model, massive igneous outpouring occurs upon initiation of a hotspot track (Richards et al., 1989). Laboratory experiments (Whitehead and Luther, 1975; Olson et al., 1988) have suggested that a large head can develop on an ascending diapir, giving rise to a flooding event when it punctures the lithosphere; present-day hotspots are then interpreted as the more sedate and steady-state expression of the tail of the mantle plume. In general, the passive model has been applied to continental flood basalts, such as the Ethiopian Traps (Courtillot et al., 1999), and the active one to oceanic plateaux. As supported by the early observations of Morgan (1972) and Winterer (1976), the active model has been proposed as the mechanism of choice for the formation of oceanic plateaux emplaced on or near a ridge (Richards et al., 1991; Winterer and Nakanishi, 1995; Gladczenko et al., 1997), and in the case of the OJP, as expressing the original phase of activity of the present-day Louisville hotspot, despite differences in geochemical signatures (Neal et al., 1997).

In the next few paragraphs, we review briefly a number of geological and geophysical properties of the OJP, as they were known mostly from investigations predating our experiment.

1.1. Age and nature of volcanism

The age of formation of the OJP is known from $^{39}Ar/^{40}Ar$ dating of basement rocks recovered at DSDP/ODP Sites 289 (on the center of the plateau) and 803 and 807 (at its northern edge) (Mahoney et al., 1993), as well as of basalt formations on Malaita, Ramos and Santa Isabel in the Solomon Islands, which are interpreted as obducted fragments of the bottom layers of the OJP (e.g., Hughes and Turner, 1977; Tejada et al., 1996). These studies suggest two episodes of emplacement: a major one at 121 ± 1 Ma, followed by a less intense one at 92 ± 2 Ma. The younger samples, found at Site 803 and on Santa Isabel, suggest that the eastern section of the OJP was formed during a later stage of volcanism (Mahoney et al., 1993; Yan and Kroenke, 1993; Parkinson et al., 1996; Kroenke and Wessel, 1997). Elaborating on this dual pulse scenario, Larson (1997) also proposed linking the Manihiki and OJ plateaux with the Nova–Canton Trough through a lateral sublithospheric ponding mechanism (Sleep, 1996).

Major element petrological signatures of the available samples are typical of oceanic tholeiites (Stoeser, 1975; Mahoney et al., 1993), and their geochemistry is that of a MORB contaminated by a hotspot source (Mahoney, 1987; Mahoney and Spencer, 1991), confirming probable on-ridge (or near-ridge) emplacement of the OJP (e.g., Nakanishi and Winterer, 1996).

1.2. Crustal structure

The OJP was targeted for crustal studies using seismic refraction in the early 1970s. Failing to detect P_n as a first arrival over profiles as long as 150 km, Furumoto et al. (1976) and Hussong et al. (1979) argued for a crustal thickness of at least 39, and possibly 45, km. These datasets were recently reinterpreted by Gladczenko et al. (1997) and complemented by a new refraction experiment involving the deployment of ocean-bottom seismometers (Miura et al., 1997).

Similarly, anomalous values of crustal thickness have been reported along other oceanic structures, such as the Tuamotu Plateau (25–32 km, Talandier and Okal, 1987), the Iceland–Færœ Ridge (25–30 km, Bott and Gunnarsson, 1980), or the Nazca Ridge (18 km, Woods and Okal, 1994), all features generally interpreted as having been generated on or near a mid-oceanic ridge.

On the other hand, and since such crustal thickness is more typical of continental structures, Nur and Ben-Avraham (1982) have speculated that oceanic plateaux, and in particular the OJP, could be wandering pieces of a lost continent. This, however, is contradicted by the basaltic nature of the drilled and obducted samples, and by the crustal stratigraphy revealed by the refraction campaigns, which is found to be typically oceanic, except for a general thickening by a factor of ~ 5 (Hussong et al., 1979; Gladczenko et al., 1997), and, hence, the continental model is now abandoned.

1.3. Geoid

The OJP has only a minor signature in the geoid, indicating a large degree of isostatic compensation.

The geoid-to-topography ratio of 1.65×10^{-3} reported by Sandwell and McKenzie (1989) could be accommodated by a 25-km thick crust, this ratio being intermediate between those of other oceanic plateaux (Manihiki: 0.52×10^{-3}; Tuamotu: 0.69×10^{-3}) and mid-plate hotspot swells (Hawaii: 3.76×10^{-3}; Tahiti: 2.47×10^{-3}). Recently, and posterior to our deployment, the joint inversion by Gladczenko et al. (1997) of the reexamined 1970 refraction data and of new gravity data yielded a crustal thickness of 36 km along the deepest section of the OJP transects.

1.4. Heat flow

Twenty-five values of heat flow measurements are available on the OJP, principally in its westcentral section (C.A. Stein, personal communication, 1999). They range from 0.4 to 1.9 HFU (17–80 mW/m^2), with an average of 1.1 HFU (47 mW/m^2). These values do not reveal any systematic heat flow anomaly over the plateau, and are if anything, lower than in the nearby Nauru Basin to the northeast (on the average of 1.25 HFU or 52 mW/m^2).

All these previous investigations then suggest the broadly consensual model of the generation of the OJP at or near a Mid-Oceanic Ridge (the Pacific–Phoenix one according to the general reconstruction of Larson (1976)), during an outburst (probably a dual one) of plume head activity, resulting in a crustal thickness of $\sim$35 km. However, most of the evidence for this figure is largely circumstantial, providing little if any insight into any lateral heterogeneity in structure, and no resolution into the underlying mantle. This clearly warrants a more detailed seismological investigation, which is the subject of the present study.

2. The experiment: layout and deployment

Because of the scarcity and inaccessibility of islands on the OJP itself, its crustal structure could not be resolved through the now classical approach of receiver functions (e.g., Owens and Zandt, 1985). Rather, we targeted four islands around the OJP for a passive experiment using sources in the Solomon–Santa Cruz seismic belt. Besides the logistical advantage of modern communications, this approach provides a dense coverage of seismic rays across the structure, allowing the inversion of Rayleigh wave dispersion for crust and mantle structure, initially under individual seismic paths, and in a second step through a full three-dimensional tomographic experiment. We chose not to use Love waves, because of the generally stronger level of noise on horizontal components in the relevant frequency band at island sites.

2.1. Deployment

Portable PASSCAL stations using three-component STS-2 seismometers were deployed in January 1994 on the islands of Chuuk, Kosrae and Nauru. It was initially hoped to avail ourselves of the permanent POSEIDON station being installed contemporaneously at Pohnpei. Difficulties in this respect mandated the deployment of a fourth station at Pohnpei in July 1995. The four stations were shut down during the first quarter of 1996.

2.2. Siting

Chuuk (12–15 Ma) is the oldest member of the Caroline chain (Keating et al., 1984); its erosion has reached the stage of a 70-km wide lagoon in which only a few basaltic islets remain above sea level. The Station (TKK; 7.447°N, 151.887°E) was installed on the island of Moen, in an abandoned tunnel entrance located under Xavier High School, a fortress-like building originally built as a communication headquarters for the Japanese Navy during World War II.

Pohnpei (5–8 Ma) is a large circular island reaching 772 m above sea level. Most of the strongly eroded interior consists of inaccessible jungle. The station (PNI; 6.969°N, 158.210°E) was deployed in an outbuilding of the Micronesian Seminar in Kolonia.

Kosrae (1.4–2.6 Ma), the youngest member of the Caroline chain, is already strongly eroded and impenetrable in most of its interior. The station (KOS; 5.324°N, 163.009°E) was installed in an abandoned government warehouse outside Topol. In October 1995, the building was reclaimed by the State of Kosrae, and the station moved 200 m to the old radio station office.

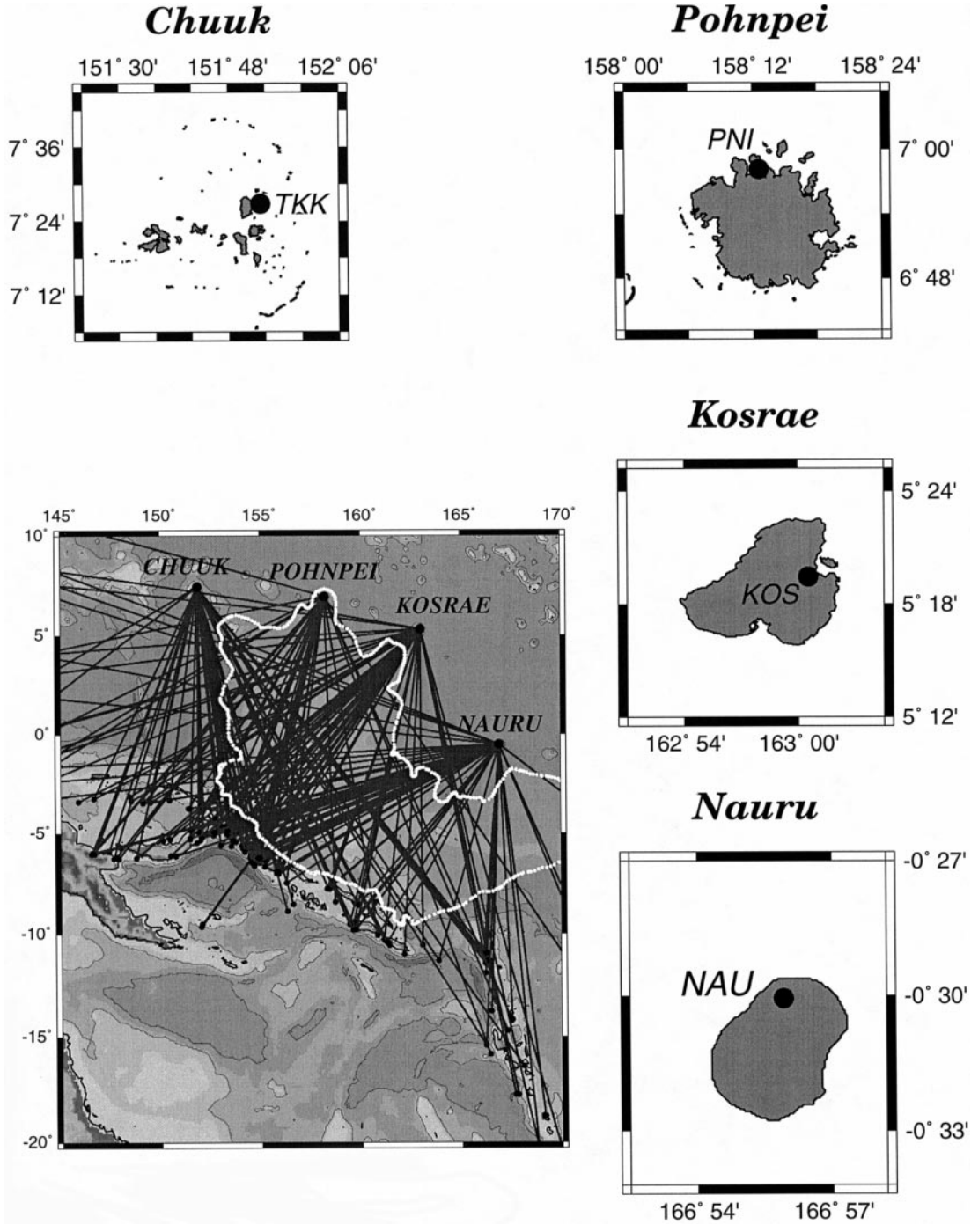

Fig. 2. Path coverage of the OJP experiment. One-dimensional inversions were carried out along each of the great-circle segments plotted, and the results subsequently inverted for the three-dimensional model. In this respect, the density of paths in any given region gives a qualitative estimate of the local resolution of the three-dimensional inversion. The plateau structure is outlined in white along the 4000-m isobath. The four small maps show the location of the four stations on their respective islands; note that the scales are different for each map.

Nauru is an uplifted atoll of unclear geological history (Hill and Jacobson, 1989), now covered with phosphate deposits, which have been mined to near exhaustion. The station (NAU; 0.509°S, 166.932°E) was deployed in a World War II Anti-Aircraft gun bunker dug into the limestone cliffs at an altitude of 60 m above sea level.

Despite several problems (flooding at Chuuk, vandalism at Nauru), the stations achieved a 77% up-time record, which must be considered good given the difficulties inherent in their operation from 11,000 km away.

2.3. Dataset

We targeted for study all earthquakes occurring in the Solomon and Vanuatu subduction systems at depths less than 210 km, and with at least one reported magnitude (m_b; M_s) above 5, resulting in the initial processing of 256 seismograms. A number of complications in the waveforms resulting from probable source complexity, as well as uncertainties in hypocentral depths (as discussed below), resulted in a final dataset of 230 seismograms inverted from 140 events, of which a full list is given by Richard-

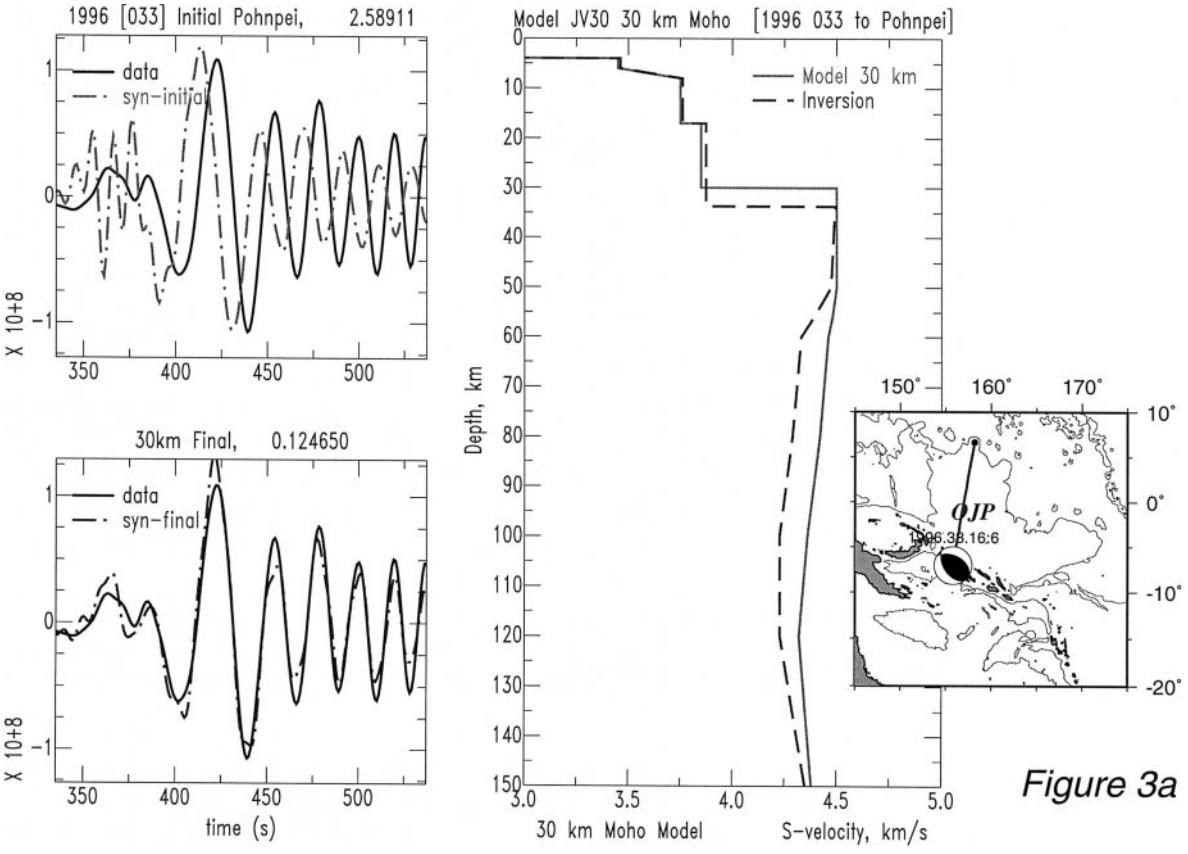

Fig. 3. (a) One-dimensional inversion for the event of 2 February 1996 in East Bougainville recorded at Pohnpei. The box at upper left shows the poor match between the observed seismogram (solid trace) and a synthetic trace computed using Model JV30 (dashed line). The bottom box shows the fit for the final model resulting from the inversion, itself described in the vertical box at right. The latter shows the shear velocity profile of the starting model (JV30; solid line) and of the final one-dimensional model for the path (dashes). Note the thicker crust (34 km) and the development of a strong low-velocity zone between 55 and 150 km. The inset summarizes the geometry of the path and of the event.

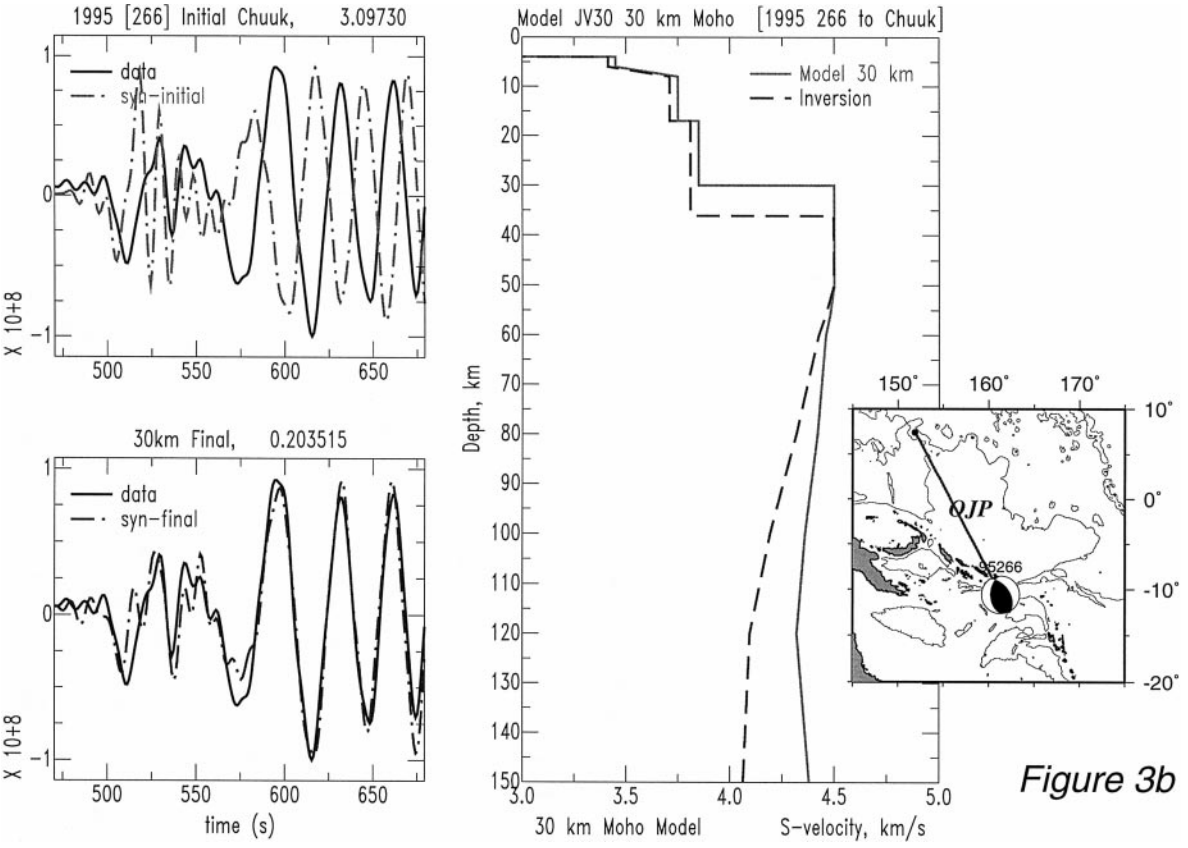

Fig. 3. (b) Same as Fig. 4a for the event of 23 September 1995 at San Cristobal, recorded at Chuuk. This model has the thickest crust among one-dimensional inversions (37 km), and a strongly developed mantle low-velocity zone.

son (1998). The spatial coverage of the OJP by the various paths is shown in Fig. 2. The time series were windowed to include arrivals between group velocities of 4.8 and 3.5 km/s, which include all body phases extending from SS to the fundamental Rayleigh wave, which can also be regarded as a complete set of Rayleigh overtones.

3. One-dimensional inversions

We first carried out one-dimensional inversions of individual records, using the first step of the partitioned waveform inversion (PWI) technique introduced by Nolet (1990), which we briefly summarize here. In this method, the local deviation from a reference Earth model $\boldsymbol{E}$ of the shear velocity along the j-th path, $\delta\beta^{(j)}(r)$, is sought as an expansion:

$$\delta\beta^{(j)}(r) = \sum_{i=1}^{M} \gamma_i^{(j)} h_i(r) \qquad (1)$$

on M basis functions h_i sampling the crust and upper mantle in a resolvable domain of depths (which in the present study we take as independent of the path j). For each path j, the vector $\boldsymbol{\gamma}^{(j)}$ is found by an inversion procedure minimizing the misfit between the observed seismogram, $d^{(j)}(t)$ and its synthetic counterpart, $s^{(j)}(t;\boldsymbol{\gamma}^{(j)})$, the latter expressed

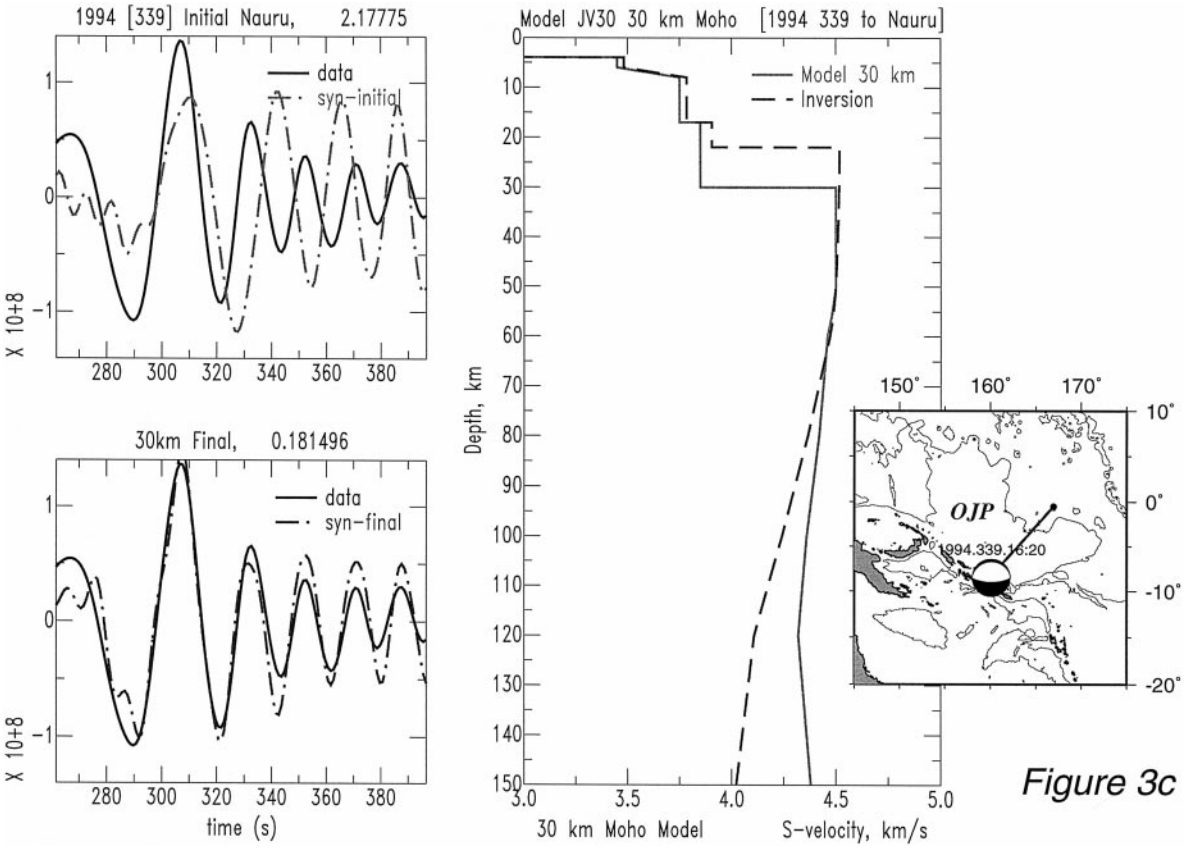

Fig. 3. (c) Same as Fig. 4a for the Guadalcanal event of 5 December 1994 recorded at Nauru. Note the much thinner crust (23 km) for this path sampling the eastern portion of the OJP.

in the frequency domain as a superposition of N surface wave modes:

$$S^{(j)}(\omega;\boldsymbol{\gamma}^{(j)}) = \sum_{n=0}^{N-1} A_{nj}^{0}(\omega)\exp\left[i\left(k_n(\omega) + \delta k_n^{j}(\omega)\right)\Delta_j\right] \quad (2)$$

where Δ_j is the epicentral distance along path j, $k_n(\omega)$ is the wavenumber of the n-th mode for the Earth model $\boldsymbol{E}$, and $\delta k_n^{j}(\omega)$ is the perturbation to $k_n(\omega)$ resulting from the change in shear velocity (1). In its simplest form, the misfit function $F^{(j)}$ would take the form:

$$F^{(j)}(\boldsymbol{\gamma}) = \int\left[s^{(j)}(t;\boldsymbol{\gamma}) - d^{(j)}(t)\right]^2 \mathrm{d}t = 2\pi\int|S^{(j)}(\omega;\boldsymbol{\gamma}) - D^{(j)}(\omega)|^2\,\mathrm{d}\omega \quad (3)$$

where Fourier transformation is expressed by capitalization. In practice, the time series $s(t)$ and $d(t)$ are subjected to filtering, and the inversion is stabilized by the addition of a Bayesian covariance term; further details can be found in the work of Nolet (1990). The procedure is then iterated until a satisfactory level of convergence is reached.

In the present study, we used $N = 30$ branches and $M = 11$ basis functions extending the perturbation to a depth of 300 km, and inverted the seismic signal in the frequency range $0.008 \le f = \omega/2\pi \le 0.125$ Hz.

3.1. Reference models

We used a variety of starting Earth models $\boldsymbol{E}$. The initial class of oceanic models, called ''OJ**'', used a constant shear velocity $\beta = 4.5$ km/s down

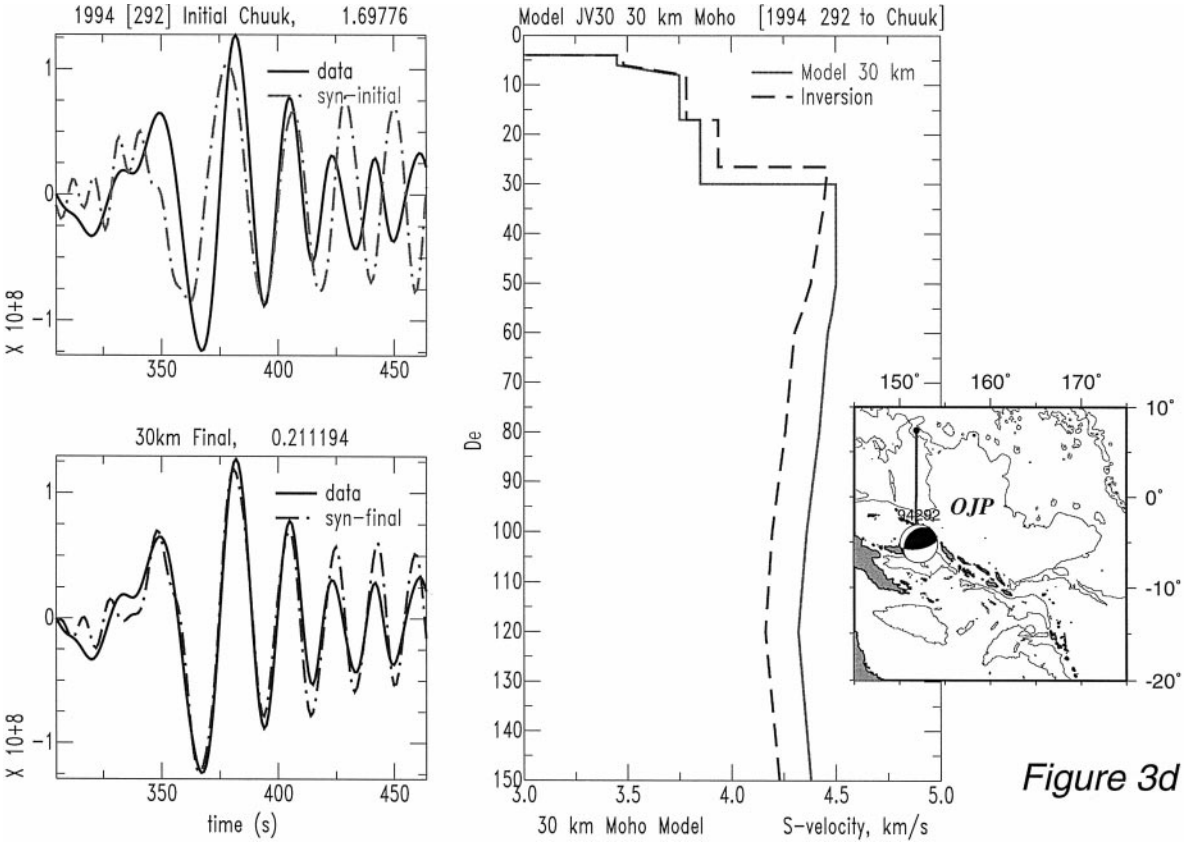

Fig. 3. (d) Same as Fig. 4a for the New Britain event of 19 October 1994, recorded at Chuuk. Note the 26-km thick crust obtained for this path crossing the Lyra Basin to the west of the OJP.

to a depth of 210 km, and the PEM-O profile (Dziewonski et al., 1975) at greater depths. These mantle models were combined with various crustal structures, with Mohorovičić [Moho] depths ranging from 15 to 45 km. For example, Model OJ30 has a 30-km-thick crust. Such variability in crustal thickness allowed a lesser degree of perturbation, and generally resulted in an improved convergence of the iterations and in reduction of residual variance. We verified, however, that the final inverted crustal thicknesses were robust with respect to a change in the starting model. The near-surface structure of the crustal models included a 3-km water column (the observed average over the OJP), a 1-km sedimentary layer, and a basaltic crust. The velocity, density and attenuation in the sedimentary structure were taken from Mosher et al. (1993). Based on early inversion models, a second class of refined models (the so-called ''JV**'' models) was developed, featuring a low-velocity zone expressed as a triangular β profile with a minimum velocity of 4.2 km/s at 120 km, together with a two-layer parameterization of the crust. The latter was introduced in the hope of recovering information on a proposed high-density cumulate in layer 3 (Neal et al., 1997). Full details of the parameterization of the various OJ** and JV** models are given in the paper of Richardson (1998).

Because the spectral phase of the seismogram is controlled primarily by the epicentral distance Δ_j in Eq. (2), source mislocation could be a serious issue in this method. Three sources of source locations were generally available: the Preliminary Determinations of Epicenters (PDE) catalogue of the National Earthquake Information Center (NEIC), the recent catalogue by Engdahl et al. (1998), and the Centroid Moment Tensor (CMT) locations of Dziewonski et

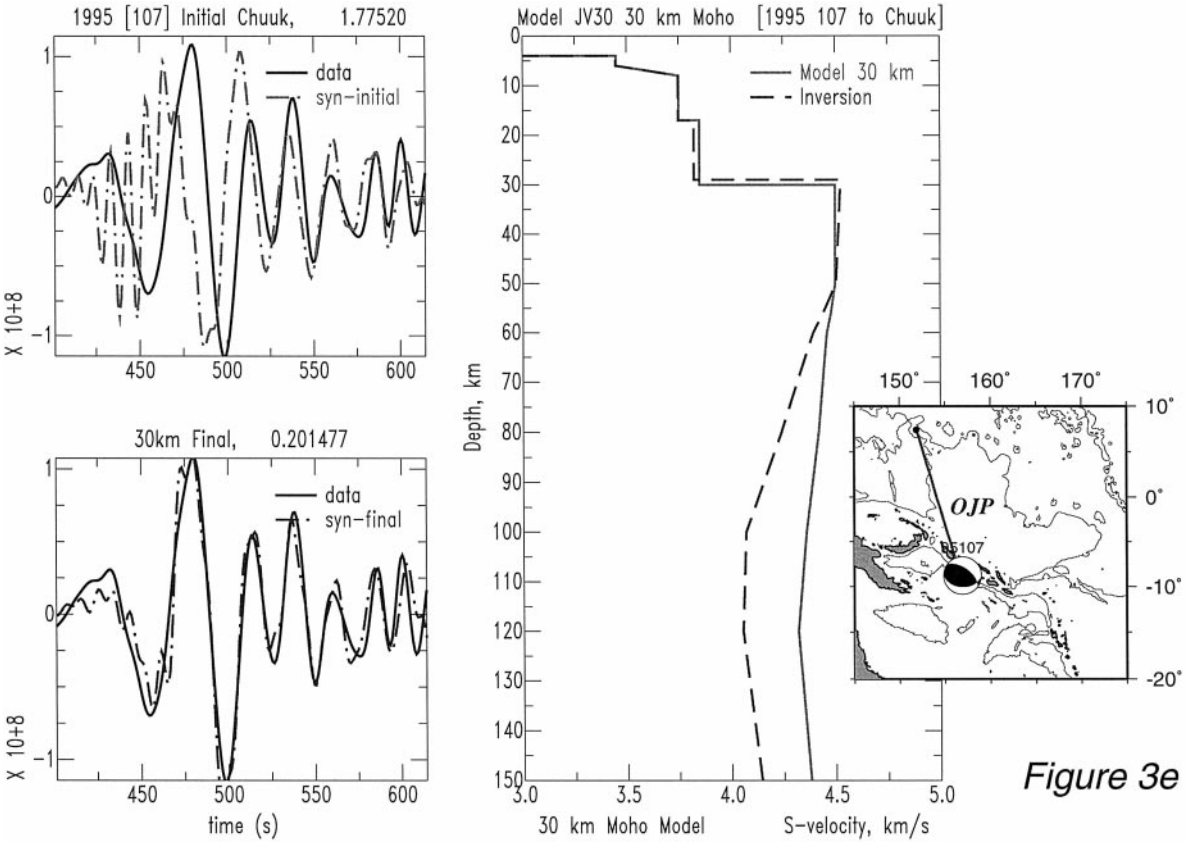

Fig. 3. (e) Same as Fig. 4a for the New Georgia event of 19 April 1995, recorded at Chuuk. The resulting model has a particularly strong low-velocity anomaly in the mantle, with β reaching 4.0 km/s at a depth of 110 km.

al. (1994) (and subsequent quarterly updates). A number of tests showed that, for the combination of path lengths and frequencies involved, the epicentral variations resulting from the use of the various catalogues were negligible factors in waveform inversions, a conclusion supported by concurrent work by Lebedev et al. (1997) and Xu and Wiens (1997).

As detailed by Nolet (1996) and Van der Lee (1998), uncertainties in depth could be significantly more challenging: first, it is well-known that the resolution of depth is poorer than that of the horizontal epicentral coordinates, with many published depth estimates remaining constrained at either 10 km (PDE, oceanic basins); 33 km (PDE, other regions) or 15 km (CMT). Second, depending on focal geometry, depth will control both the amplitude and phase excitation of the various overtones making up the seismogram; in particular (and depending on the initial model ***E*** chosen), a change in depth may move the source across the Moho discontinuity, thus strongly affecting the excitation. Our procedure was to use the PDE depth (if not constrained to 33 km), and in doubtful cases, to perform inversions for all three reported hypocenters, keeping whichever achieved the best variance reduction.

3.2. Results

These are presented in Fig. 3a–e for a variety of representative paths. In each of these figures, the boxes at left compare the observed seismograms (deconvolved ground motion; solid trace) with the

relevant synthetic for the starting model (dotted line; top) and the final inverted model (bottom). The right box compares the initial shear-velocity profile (solid line) with the final model (dashes). The inset at right sketches the geometry of the particular path involved.

The most important result, as shown in the five figures presented and confirmed on all other paths, is the extreme crustal thickness of the OJP. The average depth to the Moho discontinuity for all our paths over the OJP is 33 km, with individual values ranging from 23 to 38 km. Such very high values for the crustal thickness are however comparable to those found in such oceanic provinces as the Tuamotu Plateau (25–32 km, Talandier and Okal, 1987), the Iceland–Færœ Ridge (30–35 km, Bott and Gunnarsson, 1980), and Nazca Ridge (18 km, Woods and Okal, 1994). By analogy with such regions, this means that the OJP was formed in the immediate vicinity of a Mid-Oceanic Ridge, when the plate was still too young and hot to provide any elastic support, and the province was emplaced in a fully compensated geometry, as discussed, for example, by Cazenave and Okal (1986).

The range of values of crustal thickness found in the present study are generally less than the 35–42 km advocated by Furumoto et al. (1976), and more in line with the 32-km average of Gladczenko et al. (1997) resulting from a reinterpretation of the early seismic profiles. It should be borne in mind that our method yields an average thickness, integrated over the whole path from epicenter to station (typically 1600 km), while seismic refraction experiments were intrinsically limited to a smaller region (typically less than 200 km).

3.3. Lateral variation

Fig. 3a–e show that the crustal structure of the OJP exhibits lateral heterogeneity. The thickest crusts (38 km) are obtained for paths linking the southeastern Solomon Islands (e.g., San Cristobal) to Station TKK, and thus sampling the westcentral part of the plateau around 2°S, 157°E. To the west, the crust is found to thin to 29 km as the path samples the western border of the OJP, 26 km under the Lyra Basin (New Britain to TKK; Fig. 3d), and finally 15 km to the west of 150°E. The latter figure is in agreement with the results of Gladczenko et al. (1997) for the northeastern part of the basin in the vicinity of Chuuk (11 km), while the average figure of 23 km under the Lyra Basin essentially supports the suggestion by Kroenke (1972), Erlandson et al. (1976) and Gladczenko et al. (1997) that the OJP structure spills over into the Lyra Basin.

To the east, along the east–west branch of the OJP ''L'', crustal thicknesses of 25 ± 2 km (Fig. 3c) suggest a general thinning of the plateau structure, consistent with the suggestion of a later (90 Ma) emplacement of this portion of the structure, as also supported by the hint of a different crustal structure featuring an enhanced high-velocity layer 3 (Gladczenko et al., 1997; Neal et al., 1997). This province could have been built on somewhat mature lithosphere, capable of offering some amount of elastic support, as part of the 90-Ma reactivation of the magma source, possibly in relation to an earlier split of the plume into several discrete blobs upon ascent through the transition zone discontinuities (Bercovici and Mahoney, 1994).

3.4. Mantle structure

A common feature to all profiles inverted in this study is the development of a strong low-velocity zone between depths of 50 and at least 150 km, with shear wave speeds β dropping to as low as 3.95 km/s (Fig. 3e). This is in contrast to typical values of $\beta = 4.2$–4.3 km/s for unperturbed oceanic regions of Late Jurassic age (Mitchell and Yu, 1980; Nishimura and Forsyth, 1989), indicating that the perturbation in structure associated with the presence of the plateau reaches significantly deeper than the expected thickness of the lithospheric plate (~ 100 km).

The general level of heterogeneity revealed by the family of one-dimensional inversions warrants a full three-dimensional inversion before discussing further the nature of deeper structures.

4. Three-dimensional inversion

We apply here the second step of the PWI method of Nolet (1990) summarized below, using a slightly

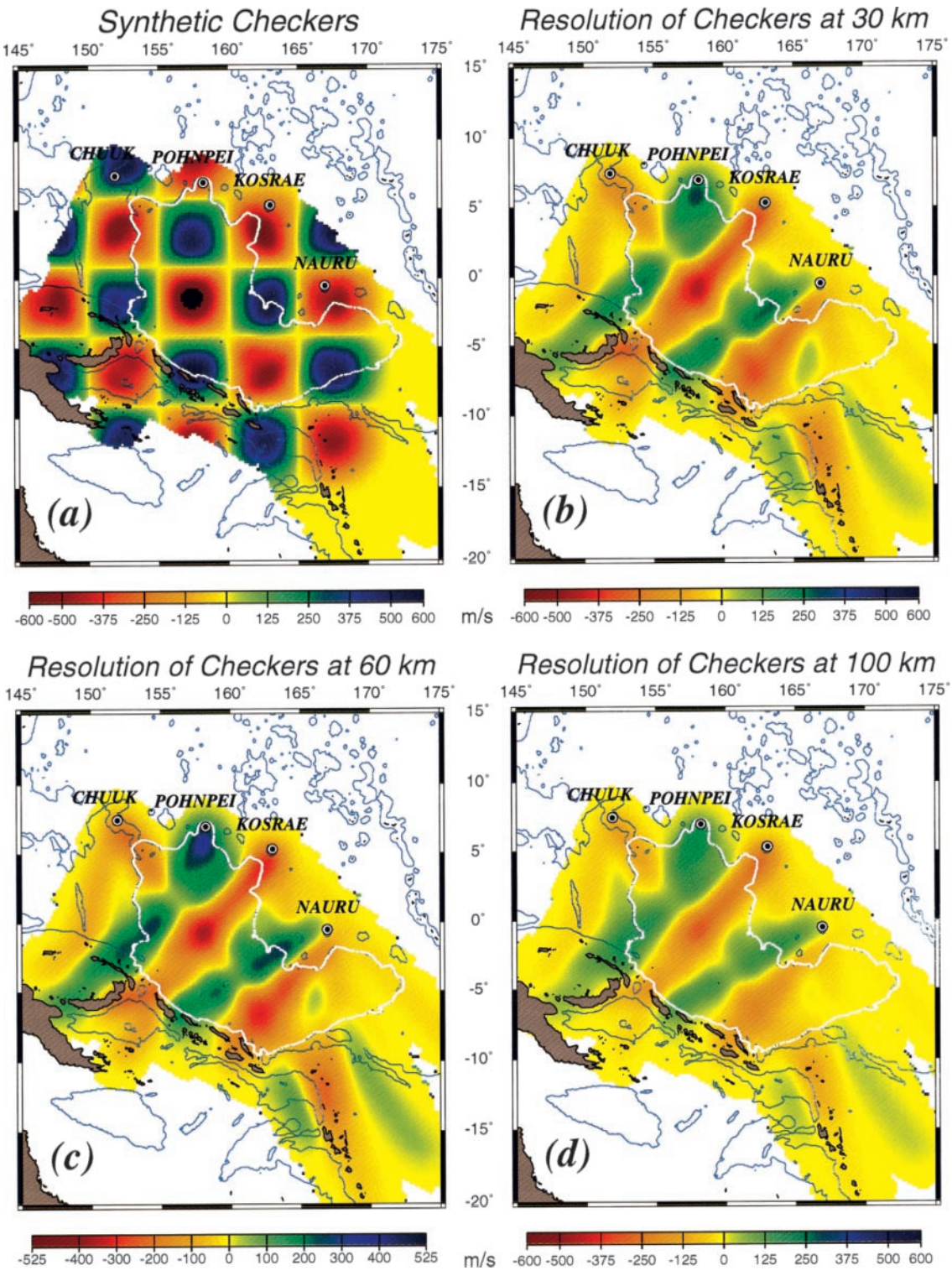
Synthetic Checkers
Resolution of Checkers at 30 km
Resolution of Checkers at 60 km
Resolution of Checkers at 100 km
CHUUK
POHNPEI
KOSRAE
NAURU
(a)
(b)
(c)
(d)
145° 150° 155° 160° 165° 170° 175°
15° 10° 5° 0° -5° -10° -15° -20°
-600 -500 -375 -250 -125 0 125 250 375 500 600
-525 -400 -300 -200 -100 0 100 200 300 400 525
m/s

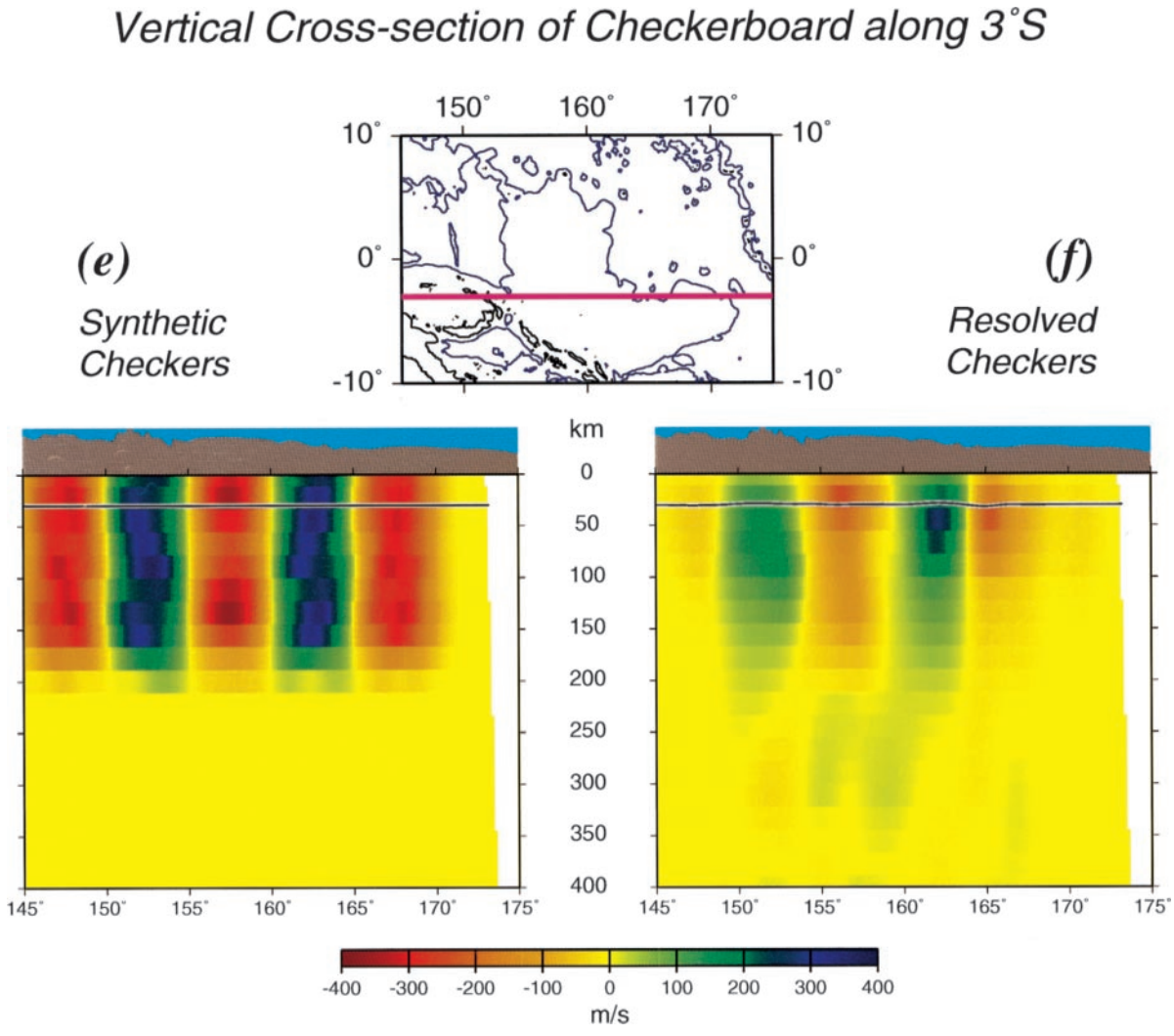

Fig. 4. Checkerboard resolution tests for the three-dimensional inversion. (a) Original checkerboard model used as input. The checkers are vertical dykes extending from the surface to 200 km. (b) Result of inversion at 30 km; note smearing along the NE–SW directions, and loss of resolution south of Nauru and in the Lyra Basin. (c) Same as (b) at 60 km depth. (d) Same as (b) at 100 km depth. (e) West–east cross-section of the checkerboard model along latitude 3°S (vertical exaggeration factor: 7); the horizontal line represents the unperturbed Moho discontinuity; a cross-section of the bathymetry is shown above the Earth structure (vertical exaggeration factor: 35). (f) Cross-section of the inverted model along the same parallel; the perturbed Moho discontinuity is also shown.

different notation, which reflects both the simplification of using a common unperturbed model (JV30) for all paths j, but, on the other hand, the additional complexity of allowing for a variable depth $H(\theta,\phi)$ to the Moho discontinuity.

We now envision a three-dimensional deviation, $\delta\beta(\boldsymbol{r}) = \delta\beta(r,\theta,\phi)$ of the shear-wave velocity from the reference model JV30. As explained by Nolet (1990), and within the domain of perturbation theory, the deviation $\delta\beta^{(j)}(r)$ found in the first step of the inversion along the j-th path, P_j, is expected to be simply the path average of the three-dimensional perturbation:

$$\delta\beta^{(j)}(r) = \frac{1}{\Delta_j}\int_{P_j}\delta\beta(r,\theta,\phi)\,\mathrm{d}\Delta \qquad (4)$$

For each of the J paths P_j, and for each of the M components of the expansion of $\delta\beta^{(j)}(r)$ onto its basis functions, Eq. (4) is equivalent to:

$$\frac{1}{a\Delta_j}\int_0^a \mathrm{d}r\ \tilde{g}_i(r)\int_{P_j}\mathrm{d}\Delta\ \delta\beta(r,\theta,\phi)=\eta_i, \qquad (5)$$

a series of $M\times J$ linear equations for the unknown model $\delta\beta(r,\theta,\phi)$. In Eq. (5), a is the Earth's radius, and the vector $\boldsymbol{\eta}$ is derived from $\boldsymbol{\gamma}$ in Eq. (1) by rotation into the principal directions of the Hessian $(\partial^2 F)/(\partial\gamma_a\partial\gamma_b)$ of the misfit function (3) at its extremum $\boldsymbol{\gamma}=\boldsymbol{\gamma}^{(j)}$. Similarly, $g_k(r)$, $\{k=1,M\}$ is rotated from $h_i(r)$, $\{i=1,M\}$, and the functions $\tilde{g}_i(r)$ are a dual basis such that:

$$\frac{1}{a}\int_0^a \tilde{g}_k(r)\,g_i(r)\mathrm{d}r=\delta_{ik} \qquad (6)$$

The final equations used in the present study,

$$\frac{1}{\Delta_j}\int_{P_j}\mathrm{d}\Delta\left[\frac{1}{a}\int_0^a\frac{\delta\beta(r,\theta,\phi)}{\sigma_\beta}\tilde{g}_i(r)\mathrm{d}r + \frac{\delta H(\theta,\phi)}{\sigma_{\mathrm{H}}}\tilde{g}_i^{\mathrm{H}}\right]=\eta_i\pm\Delta\eta_i$$

reflect the introduction of the discrete parameterization of the Moho discontinuity through its depth $H(\theta,\phi)$, and of weighting factors and error estimates in order to stabilize the inversion; details are found in the papers of Nolet (1990) and Van der Lee and Nolet (1997a).

In practical terms, the three-dimensional model $\delta\beta(r,\theta,\phi)$ is discretized along a Cartesian grid, for which we selected a 70-km spacing in the horizontal directions, and a 40-km one vertically for β. A

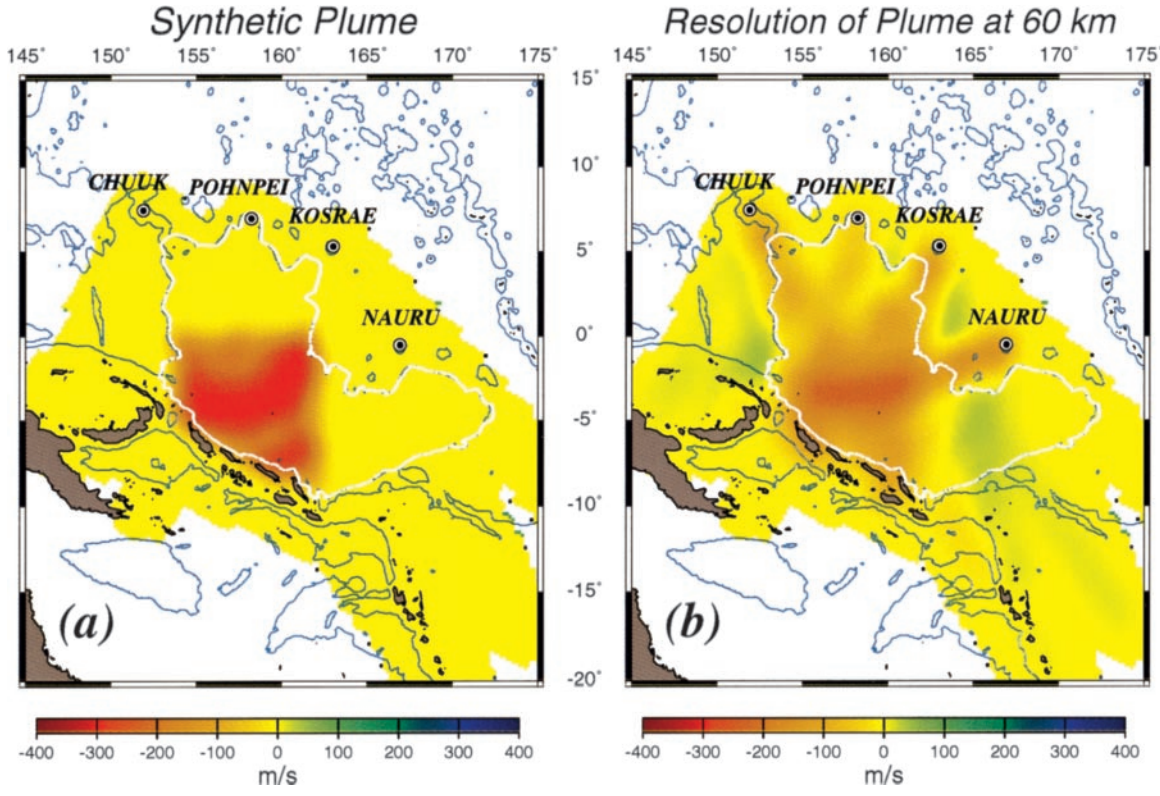

Fig. 5. Test of the resolution of a synthetic ''plume'' conceptually similar to the structure detected under the OJP. (a) Map view of the input model (at 60 km depth). (b, c and d) Same as Fig. 4c–e for the inversion of the plume model. (e and f) Same as (c) and (d) for a plume composed of depth layers alternatively fast and slow. Note the practical absence of vertical smearing.

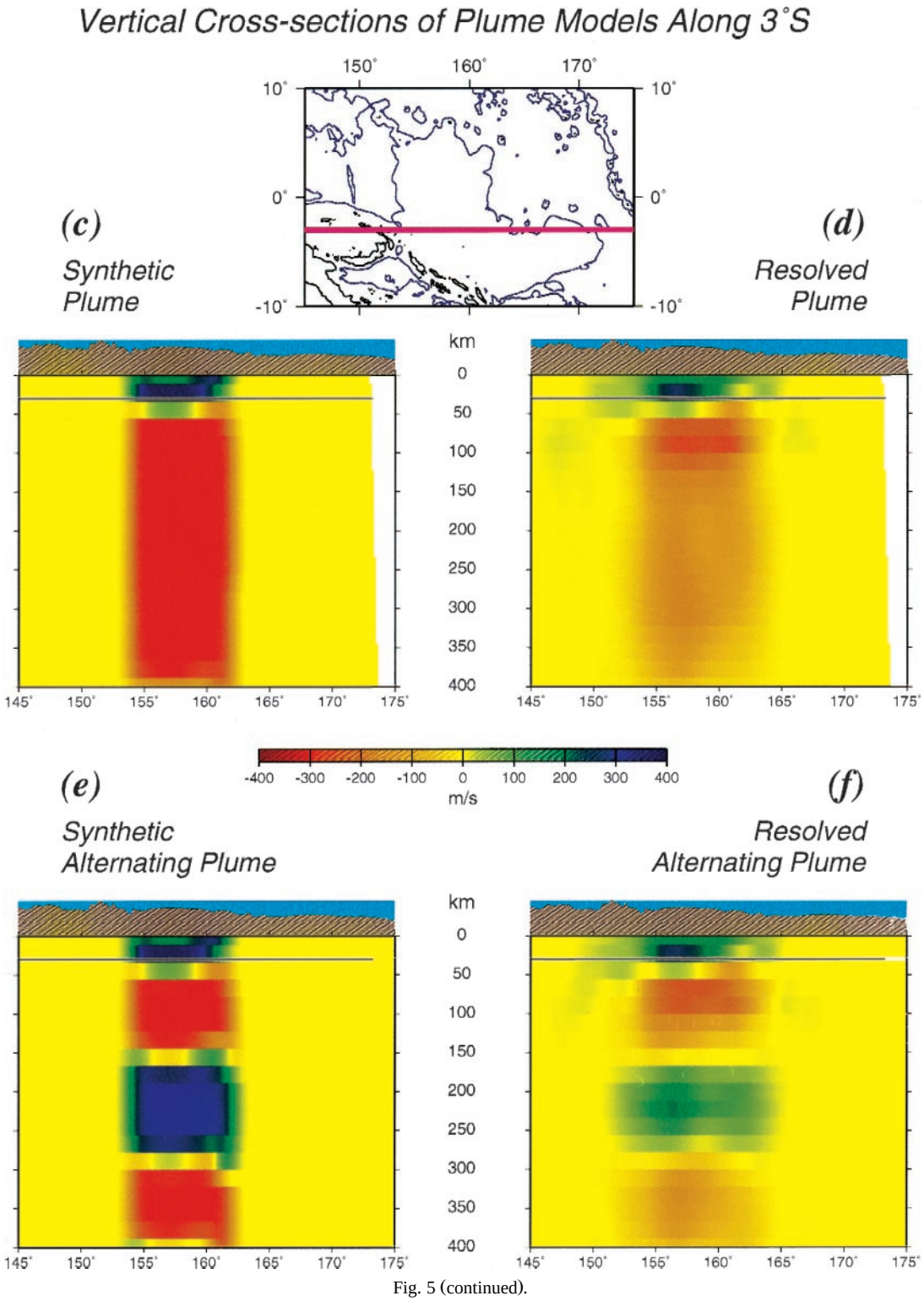

Fig. 5 (continued).

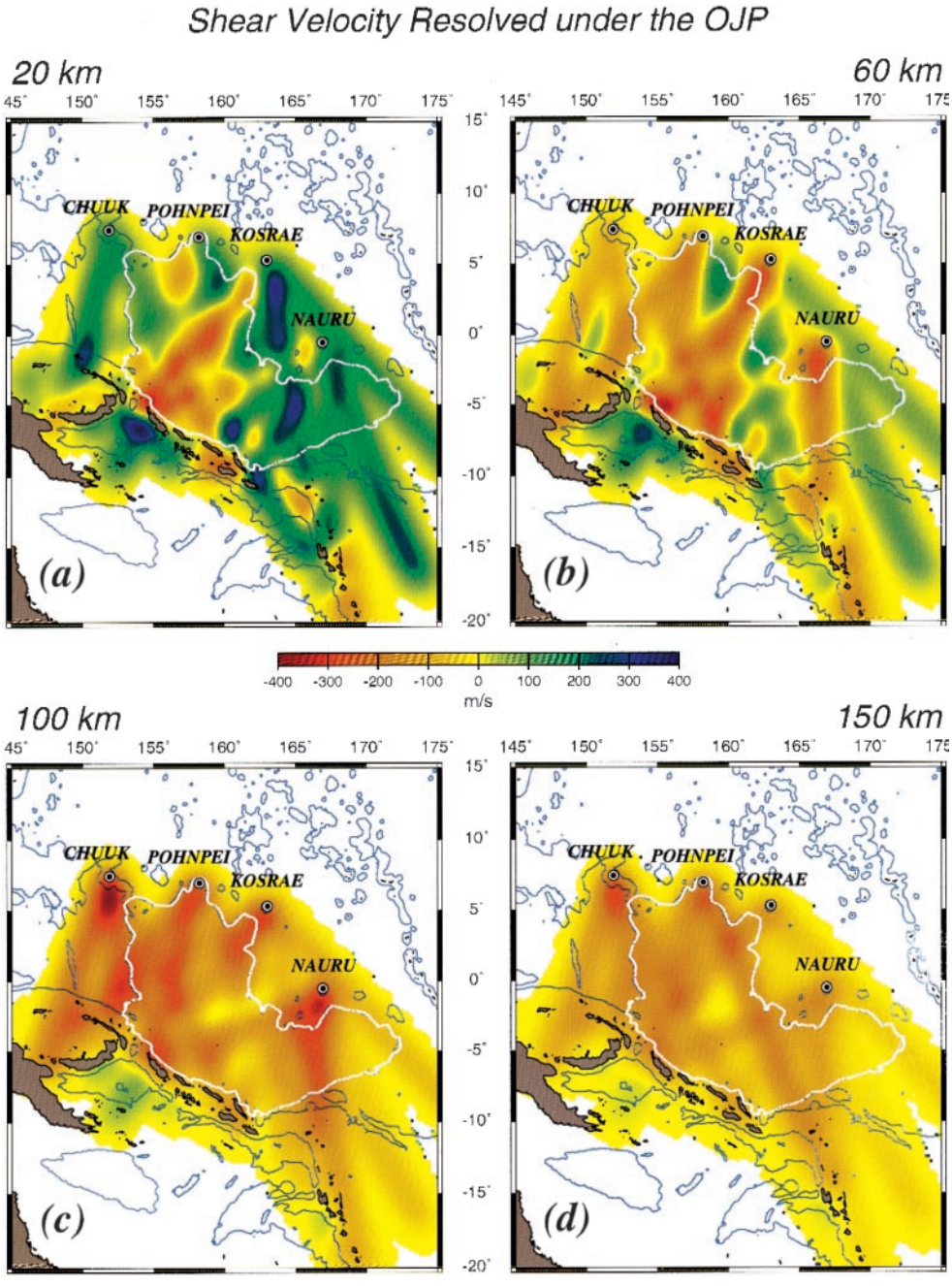

Fig. 6. Results of the inversion of the dataset shown in Fig. 2. Frames (a–d) show horizontal sections of the seismic structure of the OJP at depths of 20, 60, 100 and 150 km, respectively. Frames (e) and (f) present west–east and south–north vertical cross-sections (in the latter, the vertical exaggeration factors are 4.6 for the structure, and 23 for the bathymetric profile).

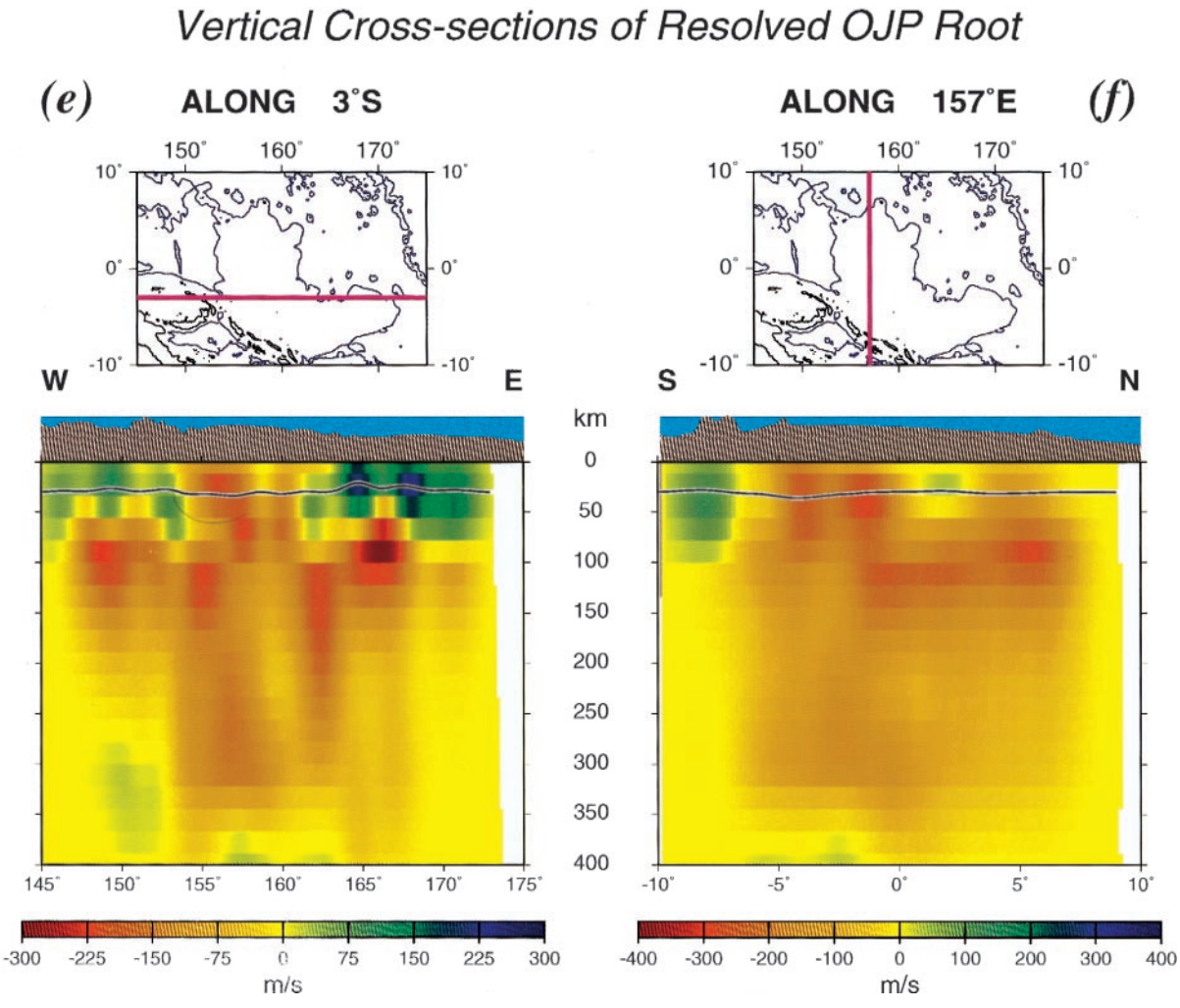

Fig. 6 (continued).

25-km vertical spacing was also tested as a verification of the stability of the inversion. The crustal thickness $H(\theta,\phi)$ is similarly discretized along a triangular tesselation on the spherical Earth.

4.1. Resolution tests

It is especially important to test the resolution of our inversion since other applications of the PWI method (e.g., Zielhuis and Nolet, 1994; Lebedev et al., 1997; Van der Lee and Nolet, 1997a,b) utilized larger datasets, especially regarding the number of receivers. We use here an asymmetric distribution where all sources are on the southern side of the structure, with a small number of stations (4), all on the northern side; the geometry of the other studies allowed a more homogeneous distribution of sources and receivers, resulting in particular in better azimuthal coverage.

Two series of resolution tests were performed. In the first one (Fig. 4), we perturbed the JV30 model with a harmonic (checkerboard) pattern centered at 60 km depth and extending from the surface to a depth of 200 km, with alternately fast and slow, square, ''dykes'' of 5° (556 km) width (Fig. 4a). The amplitude of the heterogeneity in the checkers reaches ± 0.6 km/s. The inverted structure shown here at a series of depths ranging from 30 to 100 km (Fig. 4b–d) suffers some level of smearing along the

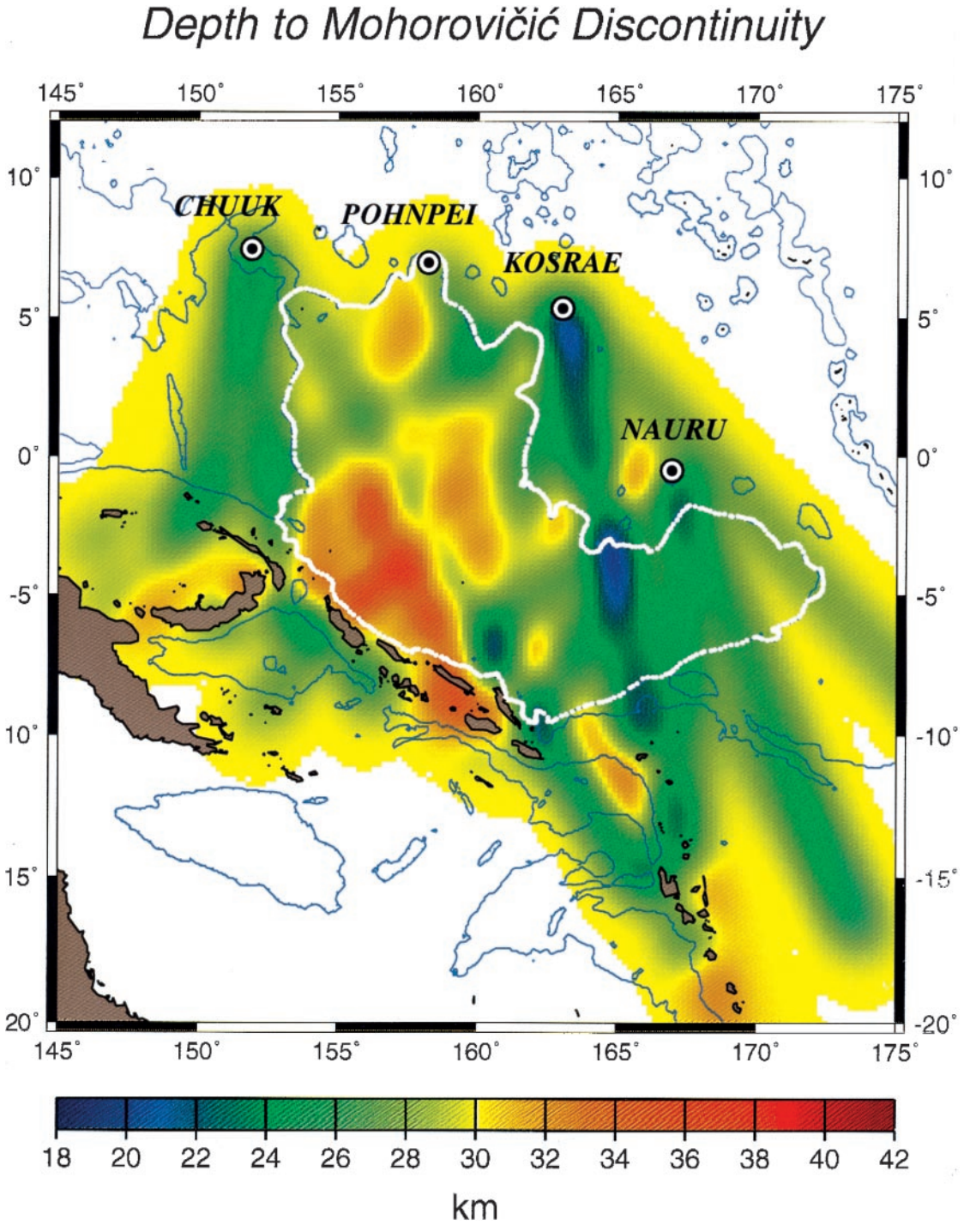

Fig. 7. Map of crustal thicknesses obtained in the three-dimensional inversion.

NE–SW direction, which is the predominant path azimuth in our dataset. In addition, and as characteristically observed in similar tests, the maximum amplitude of the model anomalies is not fully restored. Finally, and as expected, the inversion cannot resolve the frontiers of the study area, such as the easternmost tip of the OJP ''L'', where path coverage is low. However, and within these limitations, the polarity of the anomaly is recovered in a robust fashion through the most of the OJP structure, especially at the shallower depths, as illustrated in the cross-sections shown in Fig. 4e and f. We note in Fig. 4f that there is some trade-off between perturbations in shear velocity and in Moho depth: columns uniformly slow in mantle and crust result in a artificial sinking of the Moho, while fast ones yield a raised discontinuity. The amplitude of this effect is ± 2 km in the example selected.

In the second series of resolution tests (Fig. 5), we seek to reproduce a more realistic Earth structure, namely, a plug or root of the nature suggested by the one-dimensional inversions. We define the plug as a vertical dyke, centered at the bathymetric high of the plateau (4°S, 158°E), with a square cross-section of 800 km side, but limited to the southwest at the Solomon Trench. It is modeled as having a fast ($+400$ m/s) crust down to 30 km, and a slow (-400 m/s) mantle from 40 to 300 km, with a neutral layer between 30 and 40 km (Fig. 5c). Fig. 5b and d show that all three elements of the structure are well restored by the inversion, despite some lateral smearing which increases the width of the plume to 1000 km, and lessens the velocity anomaly. Finally, a vertical anomaly alternating with depth was tested (Fig. 5e–f), with the result that no significant vertical smearing could be detected for depth bands of 100 km. Fig. 5d and f suggest a depth of 300 km as a realistic bound of the resolution of the dataset.

4.2. Results

Results of the three-dimensional inversion are presented in Fig. 6. In interpreting its various frames, it should be borne in mind that they represent perturbations with respect to the JV30 model, which features a 30-km crust. Thus, in the case of the shallowest section, centered at 20 km, and with a resolution extending across the Moho discontinuity, the central, red (''slow'') cells simply confirm a crust thicker than 30 km, while the outer, green or blue (''fast'') cells indicate a crust thinner than 30 km, in agreement with the results of the one-dimensional inversions. The deeper cells centered at or below 60 km (Fig. 6b–d) indicate a uniformly slow velocity anomaly, covering the center of the plateau and reaching both into the Lyra Basin and south of Nauru at depths greater than 100 km. The cross-sections presented in Fig. 6e–f also show the resulting perturbations in Moho depth, from 21 to 34 km along the W–E section, and from 28 to 36 km along the S–N one. These fluctuations are much larger than those observed in the synthetic tests (Fig. 4f), while the perturbations in velocity are generally smaller. Also, and as shown in Fig. 7, the map of inverted crustal thickness is in general agreement with the results of the individual inversions presented in Section 3: 28–36 km along the north–south arm of the ''L'', but only 22–28 km along the east–west one.

Fig. 6e–f also confirm that the anomalous structure has the shape of a grossly cylindrical root centered around 3°S, 157°E, and approximately 600 km in radius, although this number may be enhanced by smearing artifacts. In its upper section, the structure expands sideways under the Lyra and south Nauru Basins (where the ''fast'' anomalies mapped at shallow depths simply express the thinning of the crust with respect to the reference model), and under the Caroline Islands near Pohnpei to the north. The root is present and resolved down to at least 300 km. Inverted velocity anomalies in the root are consistently -250 to -300 m/s in its upper part (above 150 km depth) and -200 m/s deeper. Since our resolution tests have generally recovered anomalies smaller in absolute value than were injected into the model, these numbers could represent a lower bound on $|\delta\beta|$, a conclusion also supported by the values obtained along individual paths in the one-dimensional inversions (e.g., Fig. 3e). In this context, we will use the figure of 5% as an order of magnitude of the low-velocity anomaly in the root.

5. Discussion and conclusion

The significant low-velocity anomaly detected under the OJP is supported by the recent global surface

wave phase velocity regionalization of Trampert and Woodhouse (1995). These authors identified a 3% deficiency in Rayleigh phase velocity over the OJP at a period of 150 s (their Fig. 5c). Even though they do not interpret their results in terms of structural anomalies at individual depths, Rayleigh kernels at this period are peaked between 150 and 300 km depth, and, thus, these authors' results are in general agreement with ours. We note, however, that Trampert and Woodhouse fail to identify a comparable anomaly in Love wave dispersion across the OJP at similar periods. In trying to reconcile these observations with ours, we note first that our lateral resolution is finer than that of Trampert and Woodhouse (1995) (on the order of 300 km, as suggested by our checkerboard tests, as opposed to 700 km in their study). In addition, fundamental Love waves are known to sample a shallower section of the Earth's structure than do Rayleigh waves of similar frequency (e.g., Dahlen and Tromp, 1998). As a result, the lateral heterogeneity in crustal structure found by our inversion (with a thick, hence, slow, central OJP and thinner, hence, faster, lateral extensions) could explain the absence of signal both in Rayleigh phase velocities at the higher frequencies, and in Love wave velocities across the spectrum in the study of Trampert and Woodhouse (1995): only at their lowest Rayleigh frequencies, will the OJP root contribute a coherent, detectable anomaly in phase velocity.

Among global tomographic studies, we note that the model S12_WM13 of Su et al. (1994) does exhibit a 1.5%–2% low-velocity signal at 200 km depth in the general area of the OJP. Other models based on spherical harmonics expansions (e.g., Li and Romanowicz, 1996) do not reveal a root to the OJP, which can be explained by their lack of resolution for a structure of such relatively small horizontal dimensions: the degree presently resolvable is $l \approx 12$, corresponding to a wavelength of 3200 km. As for body-wave investigations involving a finer, but irregular, parameterization (e.g., Grand et al., 1997; Bijwaard et al., 1998; Vasco and Johnson, 1998), they obviously suffer from a lack of sampling over a poorly instrumented region.

The existence of a low-velocity root under the OJP is supported independently by an analysis of shear-wave splitting at our four portable stations (Klosko et al., 1998). These authors document a strong deviation of the principal direction of mantle anisotropy at Chuuk (N226°E) from its expected alignment with the local azimuth of absolute plate motion (N304°E), which would be consistent with the diversion of asthenospheric mantle flow around a stiffer, impenetrable obstacle in the shape of the proposed root.

In conclusion, our 2-year passive seismic experiment across the OJP has confirmed a thick crust, averaging 33 km, but thinning out towards the sides, to 25 km at the southeastern tip of the OJP, and to 23 km under the Lyra Basin. These results confirm the probable on-ridge generation of the bulk of the plateau at 121 Ma, with a second pulse building the horizontal arm of the ''L'' in a near-ridge geometry (and, consequently, resulting in a thinner structure) at 90 Ma. More surprisingly, we detect a massive low-velocity root, extending down to a depth of 300 km, with shear wave speeds deficient by at least 250 m/s. The location of this structure under the center of the bathymetric high on the OJP is unlikely to be fortuitous, but rather, strongly suggests that this body is indeed a root of the OJP which has most probably been associated with it ever since the OJP was formed in the Cretaceous, and which must have accompanied the plateau as it drifted passively over the mantle as part of the Pacific Basin. While such deep-rooted structures have indeed been proposed for continental regions (Jordan, 1975), they had not been previously described under oceanic formations.

Other low-velocity bodies underlying LIPs were identified under the Paraná flood basalts by VanDecar et al. (1995) and under northwestern India by Kennett and Widiyantoro (1999); in both instances, these structures were associated with fossil plumes. There are however significant differences with the present study. First, the root under the OJP is much larger, extending 1200 km across as opposed to no more than 300 km; next, the perturbation in shear velocity reaches 5%, as opposed to 1.5% under India and 2.4% under Paraná (although Kennett and Widiyantoro caution that the anomaly may be stronger than reported according to their checkerboard resolution tests; different amounts of smearing in the two studies may not result in directly comparable anomalies). Finally, the OJP is attached to an oceanic plate, whereas the other sites are continental;

in the oceanic environment, we also note that a low-velocity lid, suggestive of a chemical anomaly, was found to underlie the crust of the Walvis Ridge, although no anomalously low wavespeeds were found deeper in the low-velocity zone (Chave, 1979).

We regard it as extremely unlikely that this structure could be thermally maintained. The observed 5% deficiency in β would require a temperature anomaly of 350–700 K (Duffy et al., 1995), which would easily melt the mantle and should result in massive present day volcanism, while not even a definitive high heat flow signal can be resolved. In addition, we have previously documented along the Hawaiian chain a thermal memory shorter than 20 m.y., once a plume has ceased producing active volcanism at a given location of an oceanic plate (Woods and Okal, 1996). We are thus left with the intriguing notion of a mobile keel, probably expressing a chemical heterogeneity, and traveling with the Pacific plate, as a presumed remnant of the original plume, which has failed to stay anchored in the deep mantle, in blatant violation of the Wilson paradigm.

Acknowledgements

The operation of the PASSCAL program greatly relied upon the help volunteered by many individuals, at the PASSCAL center and on the sites. In addition to thanking the wonderful people of the islands for their gracious hospitality, we are particularly indebted to Frs. Jim Croghan and Patrick Sullivan and Mr. Mike Toolan (Chuuk), Frs. Greg Muckenhaupt and Francis Hezel (Pohnpei), Mr. Lugo Skilling (Kosrae), Frs. Bernhard Lahn and Bernhard Braun and Mr. Lionel Aingimea (Nauru), for their logistical support, and for regular data retrieval and maintenance. Robert Busby and Paul Friberg (ex-PASSCAL, Palisades, NY) provided invaluable technical support. Guust Nolet suggested the use of the PWI method, and extended hospitality to WPR at Princeton, where Sergei Lebedev also provided help and support. Discussions with Ray Russo and Craig Bina are acknowledged. We thank Carol Stein for providing and discussing a file of regional heat flow data. Many figures were drafted using GMT software (Wessel and Smith, 1991). The PASSCAL project in Micronesia was supported by the National Science Foundation, under grant EAR-93-16396.

References

Arthur, M.A., Kump, L.R., Dean, W.E., Larson, R.L., 1991. Superplume, supergreenhouse?. EOS Trans. Am. Geophys. Union 72 (17), 301, abstract.

Bercovici, D., Mahoney, J.J., 1994. Double flood basalts and plume head separations at the 660-km discontinuity. Science 266, 1367–1369.

Bijwaard, H., Spakman, W., Engdahl, E.R., 1998. Closing the gap between regional and global travel-time tomography. J. Geophys. Res. 103, 30055–30078.

Bott, M.H.P., Gunnarsson, K., 1980. Crustal structure of the Iceland–Færœ Ridge. J. Geophys. 47, 221–227.

Cazenave, A., Okal, E.A., 1986. Use of satellite altimetry in studies of the oceanic lithosphere. In: Anderson, A.J., Cazenave, A. (Eds.), Space Geodesy and Geodynamics. Academic Press, London, pp. 347–375.

Chave, A.D., 1979. Lithospheric structure of the Walvis Ridge from Rayleigh wave dispersion. J. Geophys. Res. 84, 6840–6848.

Coffin, M.A., Eldholm, O., 1994. Large igneous provinces: crustal structure, dimensions, and external consequences. Rev. Geophys. 32, 11–36.

Courtillot, V., Jaupart, C., Manighetti, I., Tapponnier, P., Besse, J., 1999. On causal links between flood basalts and continental breakup. Earth Planet. Sci. Lett. 166, 177–195.

Dahlen, F.A., Tromp, J., 1998. Theoretical Global Seismology. Princeton Univ. Press, 1025 pp.

Duffy, T.S., Zha, C.-S., Downs, R.T., Mao, H.-K., Hemley, R.J., 1995. Elasticity of forsterite to 16 GPa and the composition of the upper mantle. Nature 378, 170–173.

Dziewonski, A.M., Hales, A.L., Lapwood, E.R., 1975. Parametrically simple Earth models consistent with geophysical data. Phys. Earth Planet. Inter. 10, 12–48.

Dziewonski, A.M., Ekström, G., Salganik, M.P., 1994. Centroid-moment tensor solutions for January–March 1994. Phys. Earth Planet. Inter. 86, 253–261.

Engdahl, E.R., Van der Hilst, R., Buland, R.P., 1998. Global teleseismic earthquake relocation with improved travel times and procedures for depth determination. Bull. Seismol. Soc. Am. 88, 744–757.

Erlandson, D.L., Orwig, T.L., Kilsgaard, G., Mussells, J.H., Kroenke, L.W., 1976. Tectonic interpretations of the East Carolina and Lyra Basins from reflection-profiling investigations. Geol. Soc. Am. Bull. 87, 453–462.

Furumoto, A.S., Webb, J.P., Odegard, M.E., Hussong, D.M., 1976. Seismic studies in the Ontong–Java Plateau. Tectonophysics 34, 71–90.

Gladczenko, T.P., Coffin, M., Eldholm, O., 1997. Crustal structure of the Ontong–Java Plateau: modeling of new gravity and existing data. J. Geophys. Res. 102, 22711–22729.

Grand, S.P., Van der Hilst, R.D., Widiyantoro, S., 1997. Global seismic tomography: a snapshot of convection in the Earth. GSA Today 7, 1–7.

Head, J.W., III, Coffin, M.L., 1997. Large igneous provinces: a planetary perspective. In: Mahoney, J.J., Coffin, M.F. (Eds.), Large Igneous Provinces — Continental, Oceanic and Planetary Flood Volcanism. Am. Geophys. Union Geophys. Monogr. 100, pp. 411–438.

Hill, P.J., Jacobson, G., 1989. Structure and evolution of Nauru Island, Central Pacific Ocean. Aust. J. Earth Sci. 36, 365–381.

Hughes, G.W., Turner, C.C., 1977. Upraised Pacific Ocean floor, southern Malaita, Solomon Islands. Geol. Soc. Am. Bull. 88, 412–424.

Hussong, D.M., Wipperman, L.K., Kroenke, L.W., 1979. The crustal structure of the Ontong–Java and Manihiki Plateaus. J. Geophys. Res. 84, 6003–6010.

Jordan, T.H., 1975. The continental tectosphere. Rev. Geophys. Space Phys. 13 (3), 1–12.

Keating, B.H., Mattey, D.P., Naughton, J., Helsley, C.E., 1984. Age and origin of Truk atoll, eastern Caroline Islands: geochemical, radiometric age and paleomagnetic evidence. Geol. Soc. Am. Bull. 95, 350–356.

Kennett, B.L.N., Widiyantoro, S., 1999. A low seismic wave-speed anomaly beneath northwestern India: a seismic signature of the Deccan plume?. Earth Planet. Sci. Lett. 165, 145–155.

Klosko, E.R., Russo, R.M., Okal, E.A., Richardson, W.P., 1998. Shear-wave splitting observations from Caroline Islands and Nauru. EOS Trans. Am. Geophys. Union 79, S209, abstract.

Kroenke, L.W., 1972. Geology of the Ontong–Java Plateau. PhD Dissertation, Univ. of Hawaii.

Kroenke, L.W., Wessel, P., 1997. Pacific plate motions between 125 and 90 Ma and the formation of the Ontong–Java Plateau. Proc. Chapman Confer. on the History and Dynamics of Global Motions, Marshall, CA, June 17–22, 1997. Am. Geophys. Union, Washington, DC, abstract.

Larson, R.L., 1976. Late Jurassic and early Cretaceous evolution of the Western Central Pacific ocean. J. Geomag. Geoelectr. 28, 219–236.

Larson, R.L., 1991. Geological consequences of superplumes. Geology 19, 963–966.

Larson, R.L., 1997. Superplumes and ridge interactions between Ontong–Java and Manihiki Plateaus and the Nova–Canton Trough. Geology 25, 779–782.

Larson, R.L., Olson, P., 1991. Mantle plumes control magnetic reversal frequency. Earth Planet. Sci. Lett. 107, 437–447.

Lebedev, S., Nolet, G., Van der Hilst, R.D., 1997. The upper mantle beneath the Philippine Sea region from waveform inversion. Geophys. Res. Lett. 24, 1851–1854.

Li, X.-D., Romanowicz, B.A., 1996. Global mantle shear velocity model developed using nonlinear asymptotic coupling. J. Geophys. Res. 101, 22245–22272.

Mahoney, J.J., 1987. An isotopic survey of the Pacific oceanic plateaus: implications of their nature and origin. In: Keating, B., Fryer, P., Batiza, R., Boehlert, G. (Eds.), Seamounts, Islands and Atolls, A Memorial to Henry William Menard. Am. Geophys. Union Monogr. 43, pp. 207–220.

Mahoney, J.J., Spencer, K.J., 1991. Isotopic evidence for the origin of the Manihiki and Ontong–Java Plateaus. Earth Planet. Sci. Lett. 104, 196–210.

Mahoney, J.J., Storey, M., Duncan, R.A., Spencer, K.J., Pringle, M., 1993. Geochemistry and geochronology of the Ontong–Java Plateau. In: Pringle, M., Sager, W., Sliter, W., Stein, S. (Eds.), The Mesozoic Pacific: Geology, Tectonics, and Volcanism. Am. Geophys. Union Geophys. Monogr. 77, pp. 233–261.

Mitchell, B.J., Yu, C.-K., 1980. Surface wave dispersion, regionalized velocity models, and anisotropy of the Pacific crust and upper mantle. Geophys. J. R. Astron. Soc. 63, 497–514.

Miura, S., Araki, E., Shinohara, M., Taira, A., Suyehiro, K., Takahashi, N., Coffin, M., Shipley, T., Mann, P., 1997. *P*-wave seismic velocity structure of the Solomon double trench arc system by ocean bottom seismograph observations. EOS Trans. Am. Geophys. Union 78 (46), F469, abstract.

Morgan, W.J., 1972. Plate motions and deep mantle convection. Geol. Soc. Am. Mem. 132, 7–22.

Morgan, W.J., 1981. Hotspot tracks and the opening of the Atlantic and Indian Oceans. In: Emiliani, C. (Ed.), The Sea, Vol. 7, pp. 443–487.

Mosher, D.C., Mayer, L.A., Shipley, T.H., Winterer, E.L., Hagen, R.A., Marsters, J.C., Bassinot, F., Wilkens, R.H., Lyle, M., 1993. Seismic stratigraphy of the Ontong–Java Plateau. Sci. Res. Ocean Drill. Prog. 130, 33–49.

Nakanishi, M., Winterer, E.L., 1996. Tectonic events of the Pacific plate related to formation of the Ontong–Java Plateau. EOS Trans. Am. Geophys. Union 77 (46), F713, abstract.

Neal, C.R., Mahoney, J.J., Kroenke, L.W., Duncan, R.A., Petterson, M.G., 1997. The Ontong–Java Plateau. In: Mahoney, J.J., Coffin, M.F. (Eds.), Large Igneous Provinces — Continental, Oceanic and Planetary Flood Volcanism. Am. Geophys. Union Geophys. Monogr. 100, pp. 183–216.

Nishimura, C.E., Forsyth, D.W., 1989. The anisotropic structure of the upper mantle in the Pacific. Geophys. J. Int. 96, 203–229.

Nolet, G., 1990. Partitioned waveform inversion and two-dimensional structure under the network of autonomously recording seismographs. J. Geophys. Res. 95, 8499–8512.

Nolet, G., 1996. A general view on the seismic inverse problem. In: Boschi, E., Ekström, G., Morelli, A. (Eds.), Seismic Modeling of Earth Structure. Editrice Compositori, Bologna, pp. 1–28.

Nur, A., Ben-Avraham, Z., 1982. Oceanic plateaus, the fragmentation of continents, and mountain building. J. Geophys. Res. 87, 3644–3661.

Olson, P.G., Schubert, G., Anderson, C., Goldman, P., 1988. Plume formation and lithosphere extension: a comparison of laboratory and numerical experiments. J. Geophys. Res. 93, 15065–15084.

Owens, T.J., Zandt, G., 1985. The response of the continental crust–mantle boundary observed on broad-band teleseismic receiver functions. Geophys. Res. Lett. 12, 705–708.

Parkinson, I., Arculus, R.J., Duncan, R.A., 1996. Geochemistry of the Ontong–Java Plateau basalt and gabbro sequences, Santa Isabel, Solomon Islands. EOS Trans. Am. Geophys. Union 77 (46), F715, abstract.

Richards, M.A., Duncan, R.A., Courtillot, V.E., 1989. Flood basalts and hotspot tracks: plume heads and tails. Science 246, 103–107.

Richards, M.A., Jones, D.L., Duncan, R.A., DePaolo, D.J., 1991. A plume initiation model for the formation of Wrangellia and other oceanic flood basalt plateaus. Science 253, 263–267.

Richardson, W.P., 1998. Surface wave tomography of the Ontong–Java Plateau: seismic probing of the largest igneous province. PhD Dissertation, Northwestern University, Evanston, IL, 191 pp.

Sandwell, D.H., McKenzie, K.R., 1989. Geoid highs versus topography for oceanic plateaus and swells. J. Geophys. Res. 94, 7403–7418.

Sleep, N.H., 1990. Hotspots and mantle plumes: some phenomenology. J. Geophys. Res. 95, 6715–6736.

Sleep, N.H., 1996. Lateral flow of hot plume material ponded at sublithospheric depths. J. Geophys. Res. 101, 28065–28083.

Stoeser, D.B., 1975. Igneous rocks from Leg 30 of the Deep Sea Drilling Project. Initial Rep. Deep Sea Drill. Proj. 30, 401–414.

Su, W.-J., Woodward, R.L., Dziewonski, A.M., 1994. Degree-12 model of shear velocity heterogeneity in the mantle. J. Geophys. Res. 99, 6945–6980.

Talandier, J., Okal, E.A., 1987. Crustal structure in the Tuamotu and Society Islands, French Polynesia. Geophys. J. R. Astron. Soc. 88, 499–528.

Tejada, M.L.G., Mahoney, J.J., Duncan, R.A., Hawkins, M.P., 1996. Age and geochemistry of basement and alkalic rocks of Malaita and Santa Isabel, Solomon Islands, southern margin of Ontong–Java Plateau. J. Petrol. 37, 361–394.

Trampert, J., Woodhouse, J.H., 1995. Global phase velocity maps of Love and Rayleigh waves between 40 and 150 seconds. Geophys. J. Int. 122, 675–690.

VanDecar, J.C., James, D.E., Assumpção, M., 1995. Seismic evidence for a fossil mantle plume beneath South America and implications for plate driving forces. Nature 378, 25–31.

Van der Lee, S., 1998. Observations and origin of Rayleigh-wave amplitude anomalies. Geophys. J. Int. 135, 691–699.

Van der Lee, S., Nolet, G., 1997a. Upper mantle *S* velocity structure of North America. J. Geophys. Res. 102, 22815–22838.

Van der Lee, S., Nolet, G., 1997b. Seismic image of the subducted trailing fragments of the Farrallon plate. Nature 386, 266–269.

Vasco, D.W., Johnson, L.R., 1998. Whole Earth structure estimated from seismic arrival times. J. Geophys. Res. 103, 2633–2671.

Wessel, P., Smith, W.H.F., 1991. Free software helps map and display data. EOS Trans. Am. Union 72, 441 and 445–446.

White, R.S., McKenzie, D.P., 1989. Magmatism at rift zones: the generation of volcanic continental margins and flood basalts. J. Geophys. Res. 94, 7685–7729.

White, R.S., McKenzie, D.P., 1995. Mantle plumes and flood basalts. J. Geophys. Res. 100, 17543–17585.

Whitehead, J.A., Luther, D.S., 1975. Dynamics of laboratory diapirs and plume models. J. Geophys. Res. 80, 715–717.

Winterer, E.L., 1976. Anomalies in the tectonic evolution of the Pacific. In: Sutton, G., Manghnani, M., Moberly, R. (Eds.), The Geophysics of the Pacific Ocean Basin and its Margins. Am. Geophys. Union Geophys. Monogr. 19, pp. 269–278.

Winterer, E.L., Nakanishi, M., 1995. Evidence for a plume-augmented abandoned spreading center on the Ontong–Java Plateau. EOS Trans. Am. Geophys. Union 76 (46), 617, abstract.

Woods, M.T., Okal, E.A., 1994. The structure of the Nazca Ridge and Sala y Gomez Seamount Chain from the dispersion of Rayleigh waves. Geophys. J. Int. 117, 205–222.

Woods, M.T., Okal, E.A., 1996. Rayleigh wave dispersion along the Hawaiian Swell: a test of lithospheric thinning by thermal rejuvenation at a hotspot. Geophys. J. Int. 125, 325–339.

Xu, Y., Wiens, D.A., 1997. Upper mantle structure of the southwest Pacific from regional waveform inversion. J. Geophys. Res. 102, 27439–27451.

Yan, C.Y., Kroenke, L.W., 1993. Plate tectonic reconstruction of the Southwest Pacific, 0–100 Ma. Sci. Res. Ocean Drill. Prog. 130, 697–707.

Zielhuis, A., Nolet, G., 1994. Shear-wave velocity variations in the upper mantle beneath central Europe. Geophys. J. Int. 117, 695–715.